PCCP

PAPER

View Article Online
View Journal | View Issue

Cite this: *Phys. Chem. Chem. Phys.*, 2016, **18**, 27272

Insight into the mechanism about the initiation, growth and termination of the C–C chain in syngas conversion on the Co(0001) surface: a theoretical study†

Guangxiang Wen,[a] Qiang Wang,[b] Riguang Zhang,*[a] Debao Li[b] and Baojun Wang*[a]

Received 24th July 2016,
Accepted 23rd August 2016

DOI: 10.1039/c6cp05139a

www.rsc.org/pccp

The initiation, growth and termination mechanism of the C–C chain from syngas on the Co(0001) surface have been investigated using DFT calculations. Our results show that CH_x (x = 1–3) formation is easier than CH_3OH, both CH and CH_2 species are the dominant forms of CH_x (x = 1–3), both CH and CH_2 species dominantly interact with CHO to form CHCHO and CH_2CHO, and realizes the initial C–C chain formation. Then, CHCHO and CH_2CHO prefer to be successively hydrogenated to CH_3CHO, followed by C–O bond cleavage to give CH_3CH; subsequently, CHO insertion into CH_3CH can realize the further chain growth to form CH_3CHCHO, followed by dissociation and hydrogenation to give CH_3CHCH and CH_3CH_2CHO, respectively; further, CH_3CHCH hydrogenation or CH_3CH_2CHO dissociation *via* the C–O bond cleavage can form the CH_3CH-like species CH_3CH_2CH intermediate. Thus, the mechanism of a C–C chain growth cycle has been proposed that starts from a CH_3CH_2CH intermediate, followed by repeating the above C–C chain growth cycle *via* CH_3CH intermediates, and the C–C chain growth to higher C_{2+} hydrocarbons and oxygenates can be realized, in which RCH_2CH prefers to interact with CHO to form RCH_2CHCHO, followed by its C–O bond cleavage and its hydrogenation to form $R'CHCH$ (R' = RCH_2) and $R'CH_2CHO$ (R' = RCH_2), respectively, where $R'CHCH$ hydrogenation and C–O bond cleavage of $R'CH_2CHO$ will produce $R'CH_2CH$. Moreover, aldehyde intermediates $R'CH_2CHO$ are expected to undergo C–O bond cleavage to five $R'CH_2CH$ (R' = RCH_2) rather than its desorption and its hydrogenation to alcohol. The C–C chain termination occurs at three possible positions along the growth cycle: $R'CH_2CHO$ desorption, $R'CHCH$ with successive hydrogenation steps to alkanes or alkenes, and $R'CH_2CH$ hydrogenation to alkanes, in which the relative importance of termination of $R'CHCH$ and $R'CH_2CH$ with hydrocarbons will depend strongly on the hydrogen coverage on the metal surface. The results of this work not only illustrate the initiation, growth and termination mechanism of the C–C chain involved in FTS on the Co(0001) surface, but also serve as a basis for the rational design of other Co surfaces toward desirable higher hydrocarbons or oxygenates.

1 Introduction

For Fischer–Tropsch synthesis (FTS) that converts syngas (CO and H_2) to long-chain alkanes, mono-alkenes and oxygenates,[1–4] cobalt (Co) is a commonly used catalyst due to its low water–gas shift activity, high selectivity and activity toward higher C–C chain products, as well as its relatively low cost.[5–7] Recently, Co-based catalysts have been widely utilized in long-chain fuel synthesis,[8–10] However, the corresponding initiation, growth and termination of the C–C chain from syngas are still not fully understood, which has become a bottleneck for the rational design and optimization of industrial Co-based catalysts, as well as for the development of detailed kinetics.

Up to now, extensive studies have been carried out to explore the formation mechanism of C_{2+} oxygenates and hydrocarbons

[a] *Key Laboratory of Coal Science and Technology of Ministry of Education and Shanxi Province, Taiyuan University of Technology, No. 79 Yingze West Street, Taiyuan 030024, Shanxi, P. R. China. E-mail: zhangriguang@tyut.edu.cn, wangbaojun@tyut.edu.cn, quantumtyut@126.com; Fax: +86 351 6041237; Tel: +86 351 6018239*

[b] *State Key Laboratory of Coal Conversion, Institute of Coal Chemistry, Chinese Academy of Science, Taiyuan 030001, Shanxi, P. R. China*

† Electronic supplementary information (ESI) available: Descriptions of standard molar Gibbs free energy (Part 1), H_2 adsorption and dissociation, and species on the Co(0001) surface (Part 2), adsorptions of all possible species (Part 3), CH_x (x = 1–3) and CH_3OH formation from syngas (Part 4), the reactions related to CH_2 and CH_3 species (Part 5), the reactions related to CH_xCHO (x = 1–3) (Part 6), as well as the structures of ISs, TSs and FSs for the chain growth reactions starting from CH_3CHCHO (Part 7) have been presented in detail. See DOI: 10.1039/c6cp05139a

from syngas on Co-based catalysts,[10–16] however, there is no generally accepted mechanism for the initiation, growth and termination of the C–C chain, in which two key steps are usually involved: one is the initial surface hydrocarbon species (CH_x) formation, produced by CO direct dissociation, followed by hydrogenation (carbide mechanism), or *vice versa* (H-assisted CO dissociation mechanism); the other is initial C–C chain formation by CH_x species (i) carbene coupling to C_2H_y, and (ii) CO or CHO insertion into CH_x monomer to form C_2 oxygenates.

For surface CH_x species formation, the carbide mechanism that was initially proposed by Fischer and Tropsch[17] showed that CO dissociation is the first step, followed by the dissociated C hydrogenation to CH_x (x = 1–3) species. However, CO direct dissociation does not occur easily on the Co(0001) surface due to a high activation energy.[18,19] Meanwhile, Ojeda *et al.*[11] have shown that H-assisted CH and CH_2 formation from syngas would be completely dominant on Co(0001), in which they only considered CH formation by CHO and CHOH dissociation *via* C–O bond cleavage, CH_2 formation by CH_2O dissociation and CH hydrogenation. Density functional theory (DFT) studies by Huo *et al.*[12] have indicated that CH and CH_2 formation with H-assistance from syngas is more favorable than that by CO direct dissociation on the double-stepped Co(0001), in which CH and CH_2 formation by CHO and CH_2O direct dissociation *via* C–O bond cleavage are only considered, respectively.

For the initial C–C chain formation, various mechanisms have been proposed to account for the range of products in FTS, including a carbene coupling mechanism[20,21] and CO/CHO insertion mechanism.[14,21,22] Cheng *et al.*[13] have shown that long-chain hydrocarbons are produced *via* the carbene mechanism, and long-chain oxygenates are produced *via* the CO insertion mechanism on both flat and stepped Co(0001) surfaces. Zhao *et al.*[14] found that CHO insertion is easier than CO insertion on the Co(0001) surface. Zhuo *et al.*[15] have proposed an alternative C–C chain growth cycle on the Co(0001) surface starting with CO insertion into surface RCH groups to form RCHCO, which is subsequently hydrogenated to give RCH_2CHO, further the C–O bond scission of RCH_2CHO leads to higher hydrocarbons. Xu *et al.*[16] found that for C_2 oxygenate formation from syngas over CoCu catalyst, CO/CHO insertion into CH and CH_2 are considered as the favorable pathways for C–C chain growth. In addition, Lin *et al.*[23] theoretically investigated ethanol steam reforming on the Co(0001) surface, suggesting that CH_3CH_2O, CH_3CHO, CH_3CO, CH_3 and CO are key intermediates, which may provide essential intermediates information in C_2 oxygenates formation from syngas.

Based on the above reported studies, we can deduce that H-assisted CO dissociation for CH_x formation is more favorable, however, few studies have been focused on the detailed formation mechanism of all CH_x (x = 1–3) intermediates, as well as the comparisons of the most favored monomer. Moreover, it is still open to question whether a carbene coupling mechanism or a CO/CHO insertion mechanism is dominantly responsible for the initiation and growth of the C–C chain, as well as how the C–C chain is terminated due to the reaction complexity. As a result, a detailed investigation about CH_x (x = 1–3) formation, C–C chain growth and termination from syngas at the molecular level will not only help us better understand the underlying mechanism involved in C_{2+} oxygenates and hydrocarbons, but also serve as a basis for the selective modification of Co-based catalyst to improve the catalytic performance toward the desired products.

In this study, all possible formation pathways of CH_x (x = 1–3) species have been examined to obtain the most favorable CH_x species. Then, C_{2+} oxygenates and hydrocarbons formed *via* CH_x coupling, CO/CHO insertion into CH_x, have been investigated. Further, the initiation, growth and termination of the C–C chain have been obtained. The results are obtained using DFT calculations together with periodic slab models. Moreover, the results of this work are expected to provide a better understanding on the catalytic selectivity of the Co(0001) surface toward C_{2+} oxygenates and hydrocarbons from syngas. In addition, since syngas conversion on Co catalysts is found to be structure sensitive, our present studies can serve as a basis for the rational design of other Co surfaces toward the desired products.

2 Computational details

2.1 Surface model

It is believed that the formation of cobalt carbide (Co_2C) was observed during FTS over Co-based catalysts, Co_2C might be responsible for the direct synthesis of the high alpha alcohols, and its formation was often regarded as a sign of the catalyst deactivation.[24] Thus, the initiation, growth and termination mechanism of the C–C chain for higher hydrocarbons should be carried out over metallic Co, and only a purely metallic Co form has been investigated in this study.

Co(0001) is the most stable surface among the close-packed surfaces of hexagonal closed-packed (HCP) Co to model the Co catalyst in previous DFT studies[10–16] and in this study the Co(0001) surface is also employed. The experimental Co HCP crystal has the lattice parameter of 2.51 Å;[25] then, the unit cell of HCP Co is optimized and the optimized lattice parameter was 2.49 Å. Thus the Co(0001) surface was cleaved from the HCP unit cell with the lattice parameter of 2.49 Å.

Further, in order to avoid the interactions between the adsorbed species in the adjacent periodic slab due to the limited space, especially for the larger molecules adsorbed at the very limited adsorbed sites, the surface model should be large enough for studying all mentioned reactions. Therefore, the surface model consists of a periodic $p(3 \times 3)$ supercell with four-layers of Co atoms employed, corresponding to a low coverage of 1/9 ML. Moreover, the coverage of hydrocarbons of about 0.1 ML has been experimentally reported under FTS conditions,[26] and CH_x coverage about 0.1 ML have been determined under FTS conditions using SSITKA,[27] which are in accord with our present results of a coverage of hydrocarbon species of 1/9 ML.

In all calculations, the top two layers of Co atoms and all absorbed species are relaxed, while the bottom two layers are constrained at their bulk position. For the Co(0001) surface, there are four adsorption sites: top, bridge, Hcp and Fcc, as presented in Fig. 1. The 15 Å vacuum space along the z-direction

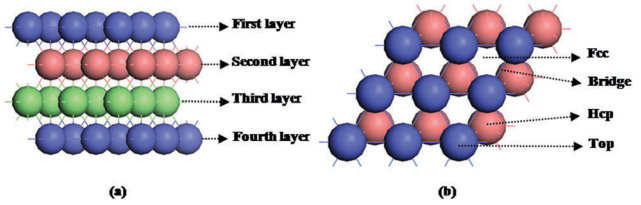

Fig. 1 The surface morphology and adsorption sites of the Co(0001) surface. (a) Side view; (b) top view.

is employed to prevent noticeable interaction between any two successive slabs. In addition, it should be also pointed out that all energies presented in this study are only valid under the low coverage, which can provide a reference for the studies at higher coverage.

2.2 Computational methods

All calculations have been carried out with the Vienna *Ab Initio* Simulation Package (VASP),[28,29] in which the electron–ion interactions are expressed by the projector-augmented wave (PAW) method.[30,31] The generalized gradient approximation (GGA) proposed by Perdew–Wang (PW91)[32] is used to describe the exchange–correlation energies and potential. All the energetics are computed with zero-point vibrational corrections in our calculation. Consideration of magnetism is essential for an accurate quantitative description of the energetics, and the magnetic properties of cobalt are thus taken into account. Thus, spin-polarized[33] DFT calculations have been included in all calculations with a plane wave cutoff energy of 400 eV. The Brillouin zone is sampled by a $5 \times 5 \times 1$ *k*-points grid generated *via* the Monkhorst–Pack procedure.[34,35] Moreover, spin-polarized calculations have also been considered for the isolated atoms and molecules in a $10 \times 10 \times 10$ Å cubic unit cell with a single *k*-point.[36] The geometry optimization will be converged when the energy differences between two electronic optimization steps are smaller than 5×10^{-6} eV, and the force is less than 0.01 eV Å^{-1}.

On the other hand, since both PAW-PBE and PAW-PW91 functionals have always been employed in the calculations that relate to Co catalyst, thus, in order to make a comparison between these two functionals, the optimized lattice constants are 2.49 Å using PAW-PBE and PAW-PW91 functionals, which agree with the experimental value (2.51 Å)[25] and other calculated values (2.51 and 2.49 Å).[11,15] Meanwhile, the adsorption energies of CO at hcp sites on the Co(0001) surface are 167.7 and 162.0 kJ mol^{-1} using PAW-PBE and PAW-PW91 functionals, respectively. Moreover, H_2 adsorption with the parallel mode at the fcc and hcp sites over the Co(0001) surface are both dissociative using either PAW-PBE or PAW-PW91 functional. Thus, the PAW-PW91 functional has been used in this study.

In addition, previous studies[37] have shown that the adsorption of the species on solid surfaces in the treatment of dispersion forces with DFT is an area where great steps forward have been made, but there are still challenges for dispersion-based DFT methods at present, as a result, it has not be considered in this study. Moreover, it is well known that DFT-D methods well describe the weak physical adsorption and the conformations of molecular clusters,[38,39] however, in the optimal pathways of C–C chain initiation, growth and termination, most of the species show strong chemisorptions, DFT-D should thus have little effect on the adsorption energies, which dominantly depend on the coverage of the adsorbed species.

To probe into the minimum energy reaction pathways, the Climbing-image Nudged Elastic Band method (CI-NEB)[40,41] is employed to find saddle points between the known reactants and products, and transition states are optimized using the dimer method.[42,43] The optimized transition state structures will be converged when the forces for all atoms are less than 0.05 eV Å^{-1}. Transition states are further confirmed by the existence of only one imaginary frequency along the proper reaction coordinates.

On the other hand, given that the contributions of zero-point vibrational energy (ZPE), thermal energy and entropy to the standard molar Gibbs free energies, the thermodynamic statistical formulas derived from partition functions have been used to correct the total energy obtained directly from DFT calculations. The standard molar Gibbs free energy for gaseous species and adsorbed species can be obtained using eqn (1):[44]

$$G^{\theta}(T,p) = E_{\text{total}} + E_{\text{ZPE}} + U^{\theta} - TS^{\theta} + \gamma RT[1 + \ln(p_{\text{CO}}/p^{\theta})] \quad (1)$$

where E_{total} refers to the total energy obtained directly from DFT calculations, R is the gas constant, p is the partial pressure of the gas-phase molecule, γ is 0 for surface adsorbed species and 1 for gaseous molecule; E_{ZPE} is the zero-point vibrational energy, U^{θ} and S^{θ} are the thermal energy and entropy, respectively. The detailed descriptions for the calculation methods of E_{ZPE}, U^{θ} and S^{θ} are presented in the Part 1 of ESI.† Moreover, since the FTS process proceeds at the temperature range of 473–623 K under realistic conditions,[45–49] as a result, all energies including adsorption free energy, reaction activation free energy and reaction free energy are calculated at a temperature of 500 K and under standard pressure in this study.

Reaction rate constants (k) are obtained in terms of TST as follows:[44,50]

$$k = \frac{k_{\text{B}}T}{h} e^{-\Delta G_{\text{a}}/RT} \quad (2)$$

Here k_{B} is the Boltzmann constant, h is the Planck constant, T is the absolute temperature, ΔG_{a} is the reaction activation free energy.

3 Results and discussion

3.1 Adsorptions of all possible species

In order to investigate the initiation, growth and termination mechanism of the C–C chain in syngas conversion, the adsorption of all possible species over four adsorption sites of the Co(0001) have been examined, only the most stable adsorption configurations are displayed in Fig. S2 (ESI†), while the adsorption free

energies at 500 K and the key structural parameters are listed in Table S1 (ESI†).

On the other hand, for H_2 adsorption and its existence form on the Co(0001) surface (see Part 2 in the ESI†), H_2 adsorption with the parallel mode at the fcc and hcp sites over the Co(0001) surface are dominantly focused on dissociative adsorption; only the single H_2 adsorption with the parallel mode at the top site is the most stable configuration of molecule adsorption, and other adsorption configurations are not favored over the Co(0001) surface. Meanwhile, for the dissociation of H_2 adsorption with the parallel mode at the top site, this reaction is exothermic (73.2 kJ mol^{-1}) with a very small activation barrier of 8.0 kJ mol^{-1}, which is rather low compared to its desorption energy (31.0 kJ mol^{-1}), previous studies by Jiang *et al.*[51] have also shown that H_2 dissociation on the Co(0001) surface has an activation barrier of about 4 kJ mol^{-1}; these results indicate that H_2 dissociation is favorable both kinetically and thermodynamically, rather than its desorption. As a result, our results can also provide a reasonable explanation for many catalytic systems related to H_2 on Co surfaces, in which all studies related to H_2 are in the form of dissociated H atoms rather than H_2 molecules. Therefore, in this study, only the interactions of the adsorbed H atom with other adsorbed species have been considered rather than H_2 molecules.

3.2 CH_x (x = 1–3) formation from syngas

Starting from CO activation, in the initial step to form C_{2+} oxygenates and hydrocarbons from syngas,[10,52] two possibilities of CH_x (x = 1–3) formation exist, one is the direct C–O bond scission of CO into C, followed by C hydrogenation to form CH_x species; the other is CO hydrogenation to form CH_xO or CH_xOH, followed by its direct or H-assisted C–O bond cleavage to form CH_x species. The corresponding activation free energies, reaction free energies, rate constants at 500 K, and the only one imaginary frequency of the transition state Co(0001) surface have been listed in Table 1, and are presented in the main text. The detailed descriptions of all elementary reactions for CH_x formation are presented in the ESI.†

3.2.1 CO activation. Three possible reactions exist for CO activation: CO direct dissociation, and CO hydrogenation to form CHO or COH, as shown in Fig. 2.

For CO direct dissociation in (R1-1), this reaction is endothermic by 85.3 kJ mol^{-1} with an activation free energy of 230.1 kJ mol^{-1}, which agrees well with other DFT values.[15,19,35] Moreover, when CO and H are co-adsorbed on the surface, CO direct dissociation in the presence of adsorbed H (R1-1′) is endothermic by 100.7 kJ mol^{-1} with an activation free energy of 232.6 kJ mol^{-1}.

For CO hydrogenation to form CHO in (R1-2), this reaction is endothermic by 120.5 kJ mol^{-1} with an activation free energy of 128.5 kJ mol^{-1}. For COH formation in (R1-3), this reaction has an activation free energy of 195.0 kJ mol^{-1}, and it is endothermic by 102.6 kJ mol^{-1}. Previous studies by Cheng *et al.*[13] and Xu *et al.*[16] agree with our calculated results.

Thus, when CO and H are co-adsorbed on the Co(0001) surface, the catalytic activity toward CO direct dissociation is rather low, CHO formation is more preferred, which has the largest reaction rate constant of 6.91×10^{-2} L mol^{-1} s^{-1}, as a result, CHO is the major product of CO activation. CH_x (x = 1–3) formation will only start with the CHO intermediate.

3.2.2 Initial CH_x (x = 1–3) formation. Starting from CHO species, CH_x (x = 1–3) formation with or without H-assistance has been discussed in detail in the ESI† (see Fig. S3–S5).

CH formation. Two reactions of CH formation without H-assistance are discussed. (R2-2) is CH formation by the C–O bond scission of CHO, (R2-3) is the C–O bond scission of CHOH formed by CHO hydrogenation. Meanwhile, two reactions of CH formation with H-assistance exist, one is C–O bond scission of CHO with H-assistance (R2-4), and the other is C–O bond scission of CHOH with H-assistance (R2-5).

As shown in Fig. S3 (ESI†), with respect to CHO and CHO + H, among four pathways of CH formation, CHO → CH + O is the most favorable pathway with activation free energy and reaction free energy of 68.9 and −62.9 kJ mol^{-1}, respectively; the reaction rate constant is 2.33×10^6 s^{-1}.

CH_2 formation. Two reactions of CH_2 formation without H-assistance exist. (R3-4) is CH_2 formation *via* the C–O bond scission of CH_2O formed by CHO hydrogenation, (R3-5) is C–O bond cleavage of CH_2OH formed by CH_2O or CHOH hydrogenation. Meanwhile, there are four possible reactions of CH_2 formation with H-assistance by the C–O bond scission of CHO (R3-6), CH_2O (R3-7), CHOH (R3-8) and CH_2OH (R3-9), respectively.

From Fig. S4 (ESI†), with respect to CHO + H, the pathway of CHO + 2H → CH_2O + H → CH_2 + OH has the lowest overall activation free energy of 84.9 kJ mol^{-1} with the reaction free energy of −20.9 kJ mol^{-1}. The corresponding rate-limiting step is CH_2O + H → CH_2 + OH with an activation free energy of 63.0 kJ mol^{-1}. However, the activation free energy of this step is larger than the adsorption free energy of CH_2O on the Co(0001) surface (37.3 kJ mol^{-1}), suggesting that CH_2O prefers to undergo desorption rather than CH_2O dissociation with H-assistance, as well as CH_2O hydrogenation to CH_3O and CH_2OH, with activation free energies of 50.0 and 115.7 kJ mol^{-1}. Namely, this pathway is not responsible for CH_2 formation. Thus, the pathway of CHO + 3H → CHOH + 2H → CH_2OH + H → CH_2 + H_2O with overall activation free energy and reaction free energy of 103.2 and 6.9 kJ mol^{-1} dominantly contribute to CH_2 formation.

CH_3 formation. Two reactions of CH_3 formation without H-assistance are discussed. (R4-4) is CH_3O direct dissociation to produce CH_3, (R4-5) is the C–O bond scission of CH_3OH formed by CH_3O or CH_2OH hydrogenation. Meanwhile, three reactions of CH_3 formation with H-assistance by the C–O bond scission of CH_2O (R4-6), CH_3O (R4-7) and CH_2OH (R4-8) exist.

As shown in Fig. S5 (ESI†), with respect to CHO + H, the pathway of CHO + 3H → CHOH + 2H → CH_2OH + H → CH_3 + OH has the lowest overall activation free energy of 103.2 kJ mol^{-1}, and the rate-limiting step CHO + H → CHOH has the rate constant of 7.00×10^3 L mol^{-1} s^{-1}. Thus, this pathway dominantly contributes to CH_3 formation.

Table 1 All possible elementary reactions, the corresponding activation free energy (ΔG_a, kJ mol^{-1}) and reaction free energies (ΔG, kJ mol^{-1}) at a temperature of 500 K, and the reaction rate constant (k, s^{-1} or L mol^{-1} s^{-1}) at a temperature of 500 K, as well as the only one imaginary frequency of the transition state (ν, cm^{-1}) involving syngas conversion on the Co(0001) surface Q4

Reactions		ν	ΔG_a (E_a)	ΔG (ΔE)	k^a
CO → C + O	(R1-1)	523i	230.1 (223.2)[b]	85.3 (80.1)	4.81×10^{-12}
CO + H → C + O + H	(R1-1′)	522i	232.6 (225.8)	100.7 (95.5)	8.12×10^{-13}
CO + H → CHO	(R1-2)	183i	128.5 (123.6)	120.5 (118.7)	6.91×10^{-2}
CO + H → COH	(R1-3)	1498i	195.0 (190.7)	102.6 (99.9)	9.71×10^{-9}
CHO + H → CHOH	(R2-1)	1367i	103.2 (99.8)	29.1 (30.9)	7.00×10^{3}
CHO → CH + O	(R2-2)	445i	68.9 (64.5)	−62.9 (−65.3)	2.33×10^{6}
CHOH → CH + OH	(R2-3)	434i	78.8 (73.5)	−69.0 (−72.5)	9.91×10^{4}
CHO + H → CH + OH	(R2-4)	1217i	82.8 (78.6)	−39.9 (−41.6)	2.42×10^{4}
CHOH + H → CH + H_2O	(R2-5)	917i	60.3 (56.1)	−19.6 (−21.3)	5.42×10^{6}
CHO + H → CH_2O	(R3-1)	815i	47.4 (43.9)	21.9 (22.9)	2.50×10^{8}
CH_2O + H → CH_2OH	(R3-2)	1232i	115.7 (113.0)	37.0 (43.0)	4.41×10^{1}
CHOH + H → CH_2OH	(R3-3)	805i	66.0 (62.9)	29.8 (35.0)	4.90×10^{6}
CH_2O → CH_2 + O	(R3-4)	449i	97.2 (92.1)	−59.6 (−62.6)	3.01×10^{3}
CH_2OH → CH_2 + OH	(R3-5)	317i	38.1 (28.9)	−79.8 (−86.5)	1.70×10^{9}
CHO + H → CH_2 + O[c]	(R3-6)	—	—	—	—
CH_2O + H → CH_2 + OH	(R3-7)	542i	63.0 (58.4)	−42.8 (−43.5)	2.63×10^{6}
CHOH + H → CH_2 + OH[c]	(R3-8)	—	—	—	—
CH_2OH + H → CH_2 + H_2O	(R3-9)	857i	26.2 (21.6)	−52.0 (−52.0)	6.21×10^{10}
CH_2O + H → CH_3O	(R4-1)	932i	50.0 (46.5)	−26.7 (−28.3)	1.81×10^{8}
CH_3O + H → CH_3OH	(R4-2)	1013i	137.3 (138.6)	48.8 (60.2)	8.60×10^{-1}
CH_2OH + H → CH_3OH	(R4-3)	963i	78.3 (75.5)	−14.9 (−11.1)	3.60×10^{5}
CH_3O → CH_3 + O	(R4-4)	588i	119.7 (118.2)	−49.7 (−49.8)	3.92×10^{0}
CH_3OH → CH_3 + OH	(R4-5)	291i	131.1 (129.4)	−75.1 (−81.4)	4.03×10^{1}
CH_2O + H → CH_3 + O	(R4-6)	414i	97.4 (92.6)	−76.4 (−78.1)	1.38×10^{3}
CH_3O + H → CH_3 + OH[c]	(R4-7)	—	—	—	—
CH_2OH + H → CH_3 + OH	(R4-8)	554i	32.0 (28.5)	−90.0 (−92.5)	1.48×10^{10}
CH → C + H	(R5-1)	825i	93.8 (92.6)	31.1 (30.5)	1.19×10^{3}
CH + H → CH_2	(R5-2)	735i	50.9 (50.2)	30.1 (31.0)	3.22×10^{6}
CH + CH → C_2H_2	(R5-3)	460i	76.3 (74.1)	−48.1 (−47.9)	1.48×10^{5}
CH + CO → CHCO	(R5-4)	290i	104.3 (95.1)	53.4 (46.0)	1.10×10^{2}
CH + CHO → CHCHO	(R5-5)	422i	56.6 (52.6)	−15.0 (−11.0)	2.72×10^{7}
CH_2 → CH + H	(R5-6)	735i	20.8 (19.2)	−29.9 (−31.0)	2.52×10^{10}
CH_2 + H → CH_3	(R5-7)	809i	50.8 (49.6)	−7.6 (−6.6)	1.15×10^{8}
CH_2 + CH_2 → C_2H_2	(R5-8)	425i	68.3 (66.7)	−39.8 (−36.1)	1.71×10^{6}
CH_2 + CO → CH_2CO	(R5-9)	371i	87.2 (80.7)	59.0 (58.1)	2.46×10^{4}
CH_2 + CHO → CH_2CHO	(R5-10)	368i	33.3 (28.9)	−24.6 (−23.1)	6.96×10^{9}
CH_3 → CH_2 + H	(R5-11)	807i	58.4 (56.2)	8.4 (6.6)	1.17×10^{7}
CH_3 + H → CH_4	(R5-12)	919i	98.9 (99.7)	2.6 (11.2)	3.99×10^{3}
CH_3 + CH_3 → C_2H_6	(R5-13)	399i	150.4 (147.8)	−23.0 (−4.4)	6.18×10^{-3}
CH_3 + CO → CH_3CO	(R5-14)	442i	141.7 (139.7)	59.0 (62.8)	1.11×10^{-1}
CH_3 + CHO → CH_3CHO	(R5-15)	415i	100.5 (96.6)	12.4 (19.1)	1.52×10^{3}
CH + CH_2 → CH_2CH	(R5-16)	495i	73.8 (71.1)	−7.1 (−5.2)	3.25×10^{5}
CHCHO + H → CH_2CHO	(R6-1)	814i	24.5 (19.7)	−58.7 (−57.6)	7.53×10^{10}
CHCHO + H → CHCHOH	(R6-2)	177i	116.9 (110.6)	27.9 (25.4)	2.35×10^{1}
CHCHO + H → $CHCH_2O$[c]	(R6-3)	—	—	—	—
CHCHO → CHCH + O	(R6-4)	420i	151.0 (143.9)	−34.9 (−39.9)	1.16×10^{-2}
CH_2CHO + H → CH_3CHO	(R6-5)	169i	57.5 (55.1)	34.0 (39.9)	1.41×10^{8}
CH_2CHO + H → CH_2CHOH	(R6-6)	1235i	96.3 (91.9)	44.2 (52.3)	3.53×10^{3}
CH_2CHO + H → CH_2CH_2O[c]	(R6-7)	—	—	—	—
CH_2CHO → CH_2CH + O	(R6-8)	474i	91.9 (85.6)	−28.3 (−31.4)	2.35×10^{3}
CH_3CHO + H → CH_3CH_2O	(R6-9)	905i	65.4 (56.0)	14.9 (24.8)	2.40×10^{7}
CH_3CHO + H → CH_3CHOH	(R6-10)	1240i	117.4 (108.8)	37.8 (45.3)	6.30×10^{0}
CH_3CHO → CH_3CH + O	(R6-11)	75i	25.0 (22.8)	−56.1 (−62.0)	3.77×10^{11}
CH_3CH_2O + H → CH_3CH_2OH	(R6-12)	1051i	75.3 (70.6)	4.4 (0.4)	9.63×10^{5}
CH_3CH_2O → CH_3CH_2 + O	(R6-13)	127i	74.5 (64.2)	−85.9 (−68.9)	4.66×10^{4}
CH_3CH + H → CH_3CH_2	(R7-1)	813i	67.4 (62.8)	22.6 (24.5)	2.61×10^{6}
CH_3CH + CH → CH_3CHCH	(R7-2)	392i	106.8 (103.3)	−13.2 (−11.2)	6.09×10^{2}
CH_3CH + CH_2 → CH_3CHCH_2	(R7-3)	434i	83.6 (80.6)	−33.9 (−40.2)	1.35×10^{5}
CH_3CH + CHO → CH_3CHCHO	(R7-4)	423i	45.5 (40.2)	−53.0 (−54.0)	2.95×10^{8}

Table 1 (*continued*)

Reactions		ν	ΔG_a (E_a)	ΔG (ΔE)	k^a
$CH_3CHCHO + H \rightarrow CH_3CH_2CHO$	(R7-5)	957i	100.0 (95.5)	20.5 (25.4)	1.71×10^3
$CH_3CHCHO \rightarrow CH_3CHCH + O$	(R7-6)	470i	94.9 (90.1)	−41.9 (−35.3)	6.87×10^3
$CH_3CH_2CHO \rightarrow CH_3CH_2CH + O$	(R7-7)	158i	28.0 (19.5)	−72.9 (−78.7)	1.49×10^{11}
$CH_3CH_2CH + CHO \rightarrow CH_3CH_2CHCHO$	(R7-8)	308i	67.1 (61.2)	−45.8 (−45.4)	4.89×10^6

[a] The unit of rate constant is s^{-1} for the reaction with only one adsorbed species as reactant, or is L mol^{-1} s^{-1} for the reaction with two co-adsorbed species as reactant. [b] Values in parentheses are at 0 K. [c] Some reactions did not provide activation barriers and reaction energies, indicating that these reactions did not take place, and are denoted as blank entries.

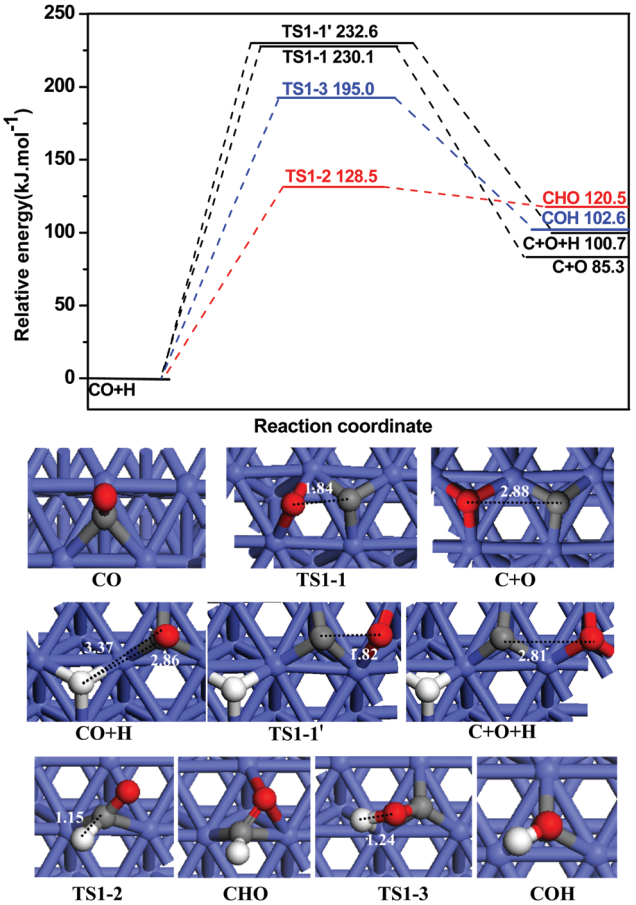

Fig. 2 The potential energy profile of CO initial activation at 500 K together with the structures of initial states, transition states and final states. Bond lengths are in Å.

3.2.3 CH_3OH formation. CH_3OH can be produced from syngas on Co-based catalysts,[53–55] thus, CH_3OH formation is examined to probe into the effect of CH_3OH on CH_x formation, as displayed in Fig. S6 (ESI†), CHO + 3H → CHOH + 2H → CH_2OH + H → CH_3OH is the most favorable formation pathway of CH_3OH.

3.2.4 Brief summary of CH_x (x = 1–3) and CH_3OH formation. The above results show that CH_x (x = 1–3) formation should start from CHO or CHO + H species. CHO → CH + O, CHO + 3H → CHOH + 2H → CH_2OH + H → CH_2 + H_2O and CHO + 3H → CHOH + 2H→ CH_2OH + H → CH_3 + OH are the optimal pathways for CH, CH_2 and CH_3 formation, respectively. CHO + 3H → CHOH + 2H → CH_2OH + H → CH_3OH is the optimal pathway for CH_3OH formation. However, starting from CHO species, CHO prefers to be dissociated into CH rather than being hydrogenated to CHOH and CH_2O, as a result, compared to CH formation by CHO dissociation, the optimal formation pathways of CH_2, CH_3 and CH_3OH *via* HCOH intermediate cannot occur easily on the Co(0001) surface. Moreover, with respect to CO + H species, as shown in Fig. 3, CH, CH_2 and CH_3 formations have overall activation free energies of 189.4, 223.7 and 223.7 kJ mol^{-1}, respectively. Therefore, taking the CHO preferable reaction and the overall activation free energy of CH_x (x = 1–3) formation into consideration, CH species is the most favorable monomer among all CH_x (x = 1–3) species on the Co(0001) surface. Meanwhile, the overall activation free energy of CH_3OH formation (257.7 kJ mol^{-1}) is much higher than CH species, indicating that CH formation is more favorable than CH_3OH, namely, the Co(0001) surface exhibits high selectivity toward CH formation.

Then, as mentioned above, since CHO is the common key intermediate for CH_x (x = 1–3) formation in FTS, CHO dissociation and hydrogenation has been examined, as a matter of fact, the isomerization reaction of CHO ↔ COH may occur, however, our results show that for the reaction of CHO → CH + O (R2-2) activation free energy barriers are 103.2, 68.9, 82.8 and 47.4 kJ mol^{-1}, respectively, which are much lower than that of the isomerization reaction CHO → COH (102.4 kJ mol^{-1}),

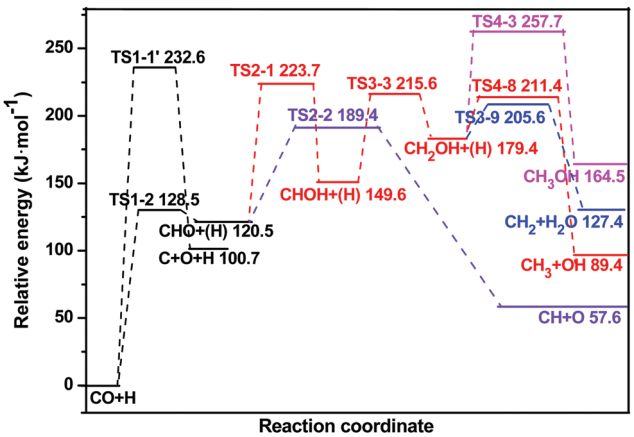

Fig. 3 The potential energy profile for the optimal paths of CH_x (x = 1–3) and CH_3OH formation from syngas with respect to CO + H species at 500 K.

suggesting that the isomerization reaction of CHO → COH is not preferable kinetically compared to the reaction of CHO → CH + O. Thus, the isomerization reaction of CHO ↔ COH has not been considered further in this study.

Further, CO direct dissociation has an activation free energy of 232.6 kJ mol^{-1}, which is much higher than the overall activation free energies of CH formation; namely, CH formation dominantly goes through H-assisted CO dissociation rather than CO direct dissociation.

3.2.5 Comparisons of CH_x (x = 1–3) formation with previous studies on Co(0001). Previous studies have investigated CH_x (x = 1–3) formation on the Co(0001) surface, Ojeda *et al.*[11] examined CH formation by CHO and CHOH direct dissociation, CH_2 formation by CH_2O direct dissociation, while CH and CH_2 formations with H-assistance, and CH_3 formation have not been discussed; Xu *et al.*[16] have studied CH_x (x = 1–3) formation by CH_xO direct dissociation, while CH_xOH direct dissociation, CH_xO and CH_xOH dissociation with H-assistance are not considered.

In our study, the pathways of CH_x (x = 1–3) formation are more detailed, for example, CH_2OH and CH_3OH direct dissociation to form CH_2 and CH_3 species are considered; further, CH_x (x = 1–3) formation with H-assistance are also examined; consequently, the most favorable pathways of CH_x formation in our study are different from those in the previous studies, for example, Xu *et al.*[16] found that CH and CH_2 species are two favorable monomers corresponding to the pathways of CHO → CH + O and CHO + H → CH_2O → CH_2 + O, respectively. However, in our study, besides CHO dissociation into CH, CHO + H → CH + OH and CHO + 3H → CHOH + 2H → CH_2OH + H → CH_2 + H_2O are also responsible for CH and CH_2 formation, respectively.

Comparing CH_x formation with other experimental and theoretical studies among different surfaces, the theoretical studies by Shetty *et al.*[52] showed that CO direct dissociation has a low activation energy of 68.0 kJ mol^{-1} on the stepped Co(10−10)-B surface, while CO hydrogenation to CHO has a higher activation energy. Liu *et al.*[56] for corrugated Co(11−21) and stepped Co(10−11) surfaces also showed that CO prefers direct dissociation rather than being hydrogenated to CHO, followed by C–O bond cleavage to form CH. Prieto *et al.*[57] have experimentally performed FTS reaction on different particle size Co/ITQ-2 catalysts, suggesting that when the particle size was decreased from 10 to 5.8 nm, CO direct dissociation into C is facile, and CH_x formation by C hydrogenation is more favorable on these defect surfaces. While Anders *et al.*[58] has found that when the particle size is larger than 6 nm, that contains more terraces, CO turnover frequency is high, which means that H-assisted CO dissociation is preferable, especially on the Co(0001) surface. The experimental studies by Yang *et al.*[59] have shown that CH_x is formed *via* H-assisted CO dissociation on the flat Co(0001) surface.

The above results indicate that CH_x formation is structure sensitive, in which H-assisted CO dissociation is dominantly responsible for CH_x formation on the flat surface. Our present results also show that CH formation mainly comes from H-assisted CO dissociation on the flat Co(0001).

3.3 Initial formation of the C–C chain

As mentioned above, CH is the predominant form among all CH_x (x = 1–3) species on the Co(0001) surface. Meanwhile, Zhao *et al.*[14] found that CHO insertion into CH_x (x = 1–3) is superior and/or competitive to CO insertion into CH_x on the Co(0001) surface. Thus, all reactions related to CH species, the dissociation, hydrogenation and coupling, as well as CO/CHO insertion have been examined.

As displayed in Fig. 4, among five reactions related to CH species, CH hydrogenation to CH_2 and CHO insertion into CH have the smallest activation free energies of 50.9 and 56.6 kJ mol^{-1}, which correspond to the large rate constants of 3.22 × 10^6 and 2.72 × 10^7 L mol^{-1} s^{-1}, respectively; thus, CH hydrogenation to CH_2 and CHO insertion into CH to CHCHO will be the most favorable pathways.

Due to the easy formation of CH_2 by CH hydrogenation, among five reactions related to CH_2 species (see Fig. S7, ESI†), CH_2 dissociation into CH and CHO insertion into CH_2 to CH_2CHO are the most favorable pathways. Moreover, of the

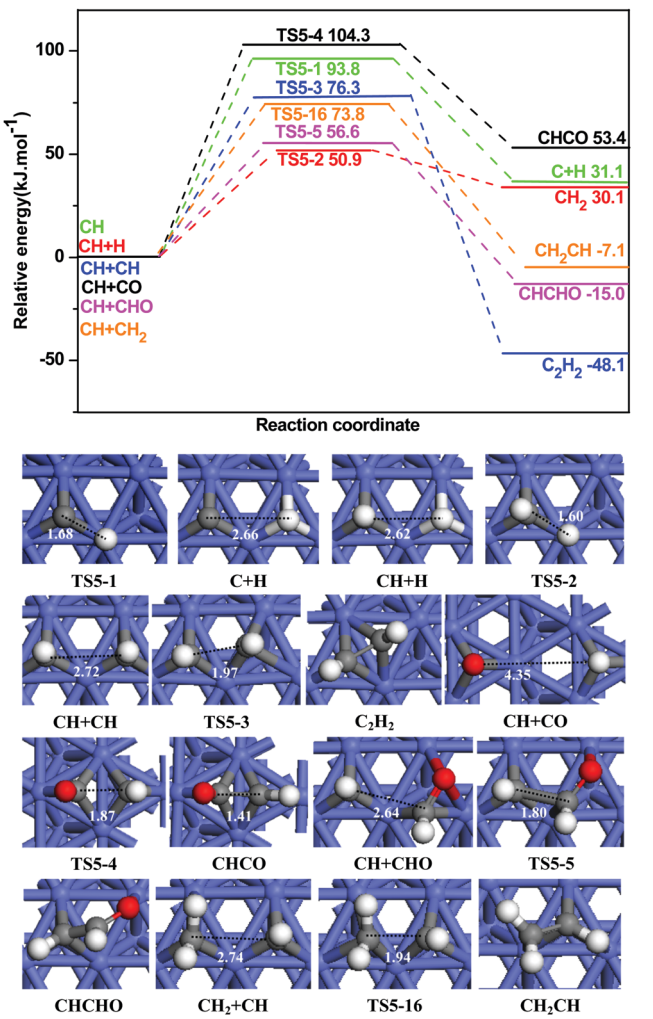

Fig. 4 The potential energy profile of CH dissociation, hydrogenation, coupling and insertion reactions at 500 K together with the structures of initial states, transition states and final states. Bond lengths are in Å.

five reactions related to CH_3 species (see Fig. S8, ESI†), CH_3 dissociation is more favorable than CH_3 hydrogenation, coupling, as well as CO/CHO insertion into CH_3, suggesting that even if CH_3 species can be produced, they will be easily dissociated into CH_2 intermediates, as a result, the possibilities of CH_3 species formation is ruled out from CH_x (x = 1–3) species over the Co(0001) surface.

On the basis of the above results, the primary forms of CH_x (x = 1–3) are CH and CH_2 species for syngas conversion on the Co(0001) surface, in which CH species arise from CHO dissociation and CH_2 species is formed by CH hydrogenation. Once CH and CH_2 species are formed, CHO insertion into CH and CH_2 species lead to C_2 oxygenates CHCHO and CH_2CHO, respectively, which realizes the initial C–C chain formation. In addition, our results show that CHO insertion into CH_x (x = 1–3) is easier than CO insertion into CH_x (x = 1–3), which agrees with the DFT results by Zhao *et al.*,[14] this may arise from the smaller HOMO–LUMO gap of CHO compared to CO, which facilitates the charge transfer and hybridization with the surface.

Further, since CH and CH_2 species are the major forms of CH_x (x = 1–3), we consider the coupling of CH with CH_2 to form the C–C chain, suggesting that the coupling of CH and CH_2 is less favorable, namely, CHO insertion into CH and CH_2 to CHCHO and CH_2CHO are more preferred to realize the initial C–C chain formation.

3.4 Growth of the C–C chain

As mentioned above, the initial C–C chain formation leads to CHCHO and CH_2CHO, which may undergo hydrogenation or dissociation *via* C–O bond cleavage, as displayed in Fig. S9 (ESI†). Meanwhile, the detailed descriptions relating to CH_xCHO reactions are presented.

From the rate constant k in Table 1 and the potential energy profile in Fig. S9 (ESI†), we can deduce that CHCHO hydrogenation to give CH_2CHO is more preferable; CH_2CHO prefers to be hydrogenated to form CH_3CHO, and CH_3CHO prefers to be dissociated into CH_3CH intermediate.

Beginning with the CH_3CH intermediate, CH_3CH hydrogenation, coupling with CH and CH_2, as well as CHO insertion (see Fig. 5) show that CHO insertion into CH_3CH to give CH_3CHCHO is the most favorable pathway both thermodynamically and kinetically, which has the largest rate constant of 2.95×10^8 L mol^{-1} s^{-1}. Thus, CH_3CHCHO will be responsible for further chain growth.

Starting from CH_3CHCHO with the stronger adsorption free energy of 156.5 kJ mol^{-1}, as shown in Table S1 and Fig. S10 (ESI†), CH_3CHCHO dissociation and hydrogenation are two parallel pathways leading to CH_3CHCH and CH_3CH_2CHO, respectively; the reactions have activation free energies of 94.9 and 100.0 kJ mol^{-1}, respectively.

Starting from the CH_3CHCH intermediate, CH_3CHCH can hydrogenate to give CH_3CH_2CH with an activation free energy of 53.2 kJ mol^{-1}, then, CHO insertion into CH_3CH_2CH will realize the chain growth. On the other hand, starting from the CH_3CH_2CHO intermediate, its C–O bond cleavage results in CH_3CH_2CH, followed by hydrogenation, the coupling with CH and CH_2, as well as CHO insertion can form C_3 and C_4 hydrocarbons or C_4 oxygenates; similarly to CH_3CHO species, CH_3CH_2CHO species also prefers to be dissociated into CH_3CH_2CH, subsequently, CHO insertion into CH_3CH_2CH will realize the chain growth. The energetics for the reactions $CH_3CH_2CHO \rightarrow CH_3CH_2CH + O$ (R7-7) and $CH_3CH_2CH + CHO \rightarrow CH_3CH_2CHCHO$ (R7-8) are calculated, suggesting that CH_3CH_2CHO dissociation has an activation free energy of 28.0 kJ mol^{-1}, and it is exothermic by 72.9 kJ mol^{-1}. Moreover, CHO insertion into CH_3CH_2CH has an activation free energy of 67.1 kJ mol^{-1}, and it is exothermic by 45.8 kJ mol^{-1}. Thus, the chain growth from C_3 to C_4 go through a similar pathway with that from C_2 to C_3, which agree with the studies by Cheng *et al.*[20]

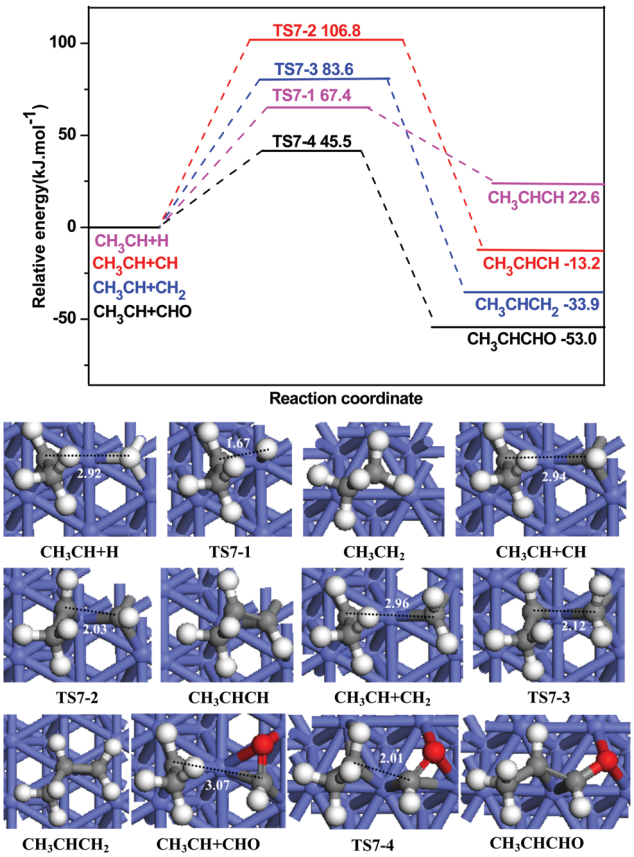

Fig. 5 The potential energy profile of CH_3CH hydrogenation, coupling and insertion reactions at 500 K together with the structures of initial states, transition states and final states. Bond lengths are in Å.

Further, C_4 hydrocarbons CH_3CH_2CHCH can be formed by the C–O bond cleavage of CH_3CH_2CHCHO, and it can be hydrogenated to $CH_3CH_2CH_2CH$, which can be also formed *via* the C–O bond cleavage of $CH_3CH_2CH_2CHO$ by CH_3CH_2CHCHO hydrogenation; subsequently, CHO insertion into $CH_3CH_2CH_2CH$ realizes the chain growth from C_4 to C_5 hydrocarbons or oxygenates.

Therefore, upon repeating the above C–C growth cycle, the growth of the C–C chain on the Co(0001) surface can be realized to form C_{2+} hydrocarbons and oxygenates; more importantly, during the C–C growth cycle, the aldehyde intermediate RCH_2CHO

is expected to undergo C–O bond cleavage to form RCH_2CH hydrocarbons rather than its desorption. Alternatively, RCHCHO with the strong adsorption free energy can also undergo C–O bond cleavage to form RCHCH, followed by its hydrogenation to form RCH_2CH, or RCHCHO undergoes hydrogenation to RCH_2CHO, followed by C–O bond cleavage to form RCH_2CH; subsequently, the RCH_2CH intermediate prefers to interact with CHO to form RCH_2CHCHO, which can be attributed to the low activation energy of CHO insertion; further, RCH_2CHCHO goes through a combination of dissociation and hydrogenation, leading to $R'CH_2CH$ ($R' = RCH_2$).

3.5 Termination of the C–C chain

For C–C chain termination, the termination can occur at different positions along the C–C chain growth cycle. Since this process involves C_{2+} hydrocarbons and oxygenates, the C–C chain termination for C_{2+} oxygenates and hydrocarbons have been discussed, respectively.

For the chain termination with aldehyde species RCH_2CHO, the C–O bond cleavage of CH_3CHO has an activation free energy of 25.0 kJ mol^{-1}, and the CH_3CHO desorption energy is 24.3 kJ mol^{-1}, indicating that CH_3CHO dissociation is energetically compatible with its desorption. Further, with the C–C chain growth, CH_3CHCHO hydrogenation to give CH_3CH_2CHO has a similar activation energies with that of C–O bond cleavage of CH_3CHCHO (100.0 *vs.* 94.9 kJ mol^{-1}), then, CH_3CH_2CHO dissociation into CH_3CH_2CH has an activation free energy of 28.0 kJ mol^{-1}, the CH_3CH_2CHO desorption energy is −5.4 kJ mol^{-1}, thus, CH_3CH_2CHO desorption is favorable.

For the chain termination with alcohol species RCH_2OH, RCH_2CHO prefers to be dissociated into RCH_2CH or undergo desorption rather than being hydrogenated to alcohols RCH_2CH_2OH, as a result, the chain termination with RCH_2CHO hydrogenation to alcohols is less preferable although the alcohols have low desorption energy. Thus, the hydrogenation of aldehyde oxygenates to form an alcohol seems unlikely due to the easy C–O bond cleavage or desorption kinetically; the C–C chain termination should focus on the desorption of aldehyde from the Co(0001) surface into gas phase due to the weak adsorption energy, which may be compatible with the activation energy of C–O bond cleavage of the aldehyde, for example, CH_3CH_2CHO has a weaker adsorption free energy of −5.4 kJ mol^{-1}, which easily desorbs from the Co(0001) surface into gas phase CH_3CH_2CHO.

For the chain termination with C_{2+} hydrocarbons, CH_3CH arises from the C–O bond cleavage of CH_3CHO, and CHO insertion into CH_3CH has a lower activation free energy than its hydrogenation to CH_3CH_2 (45.5 *vs.* 67.4 kJ mol^{-1}). Similarly, CH_3CH_2CH from the C–O bond cleavage of CH_3CH_2CHO also prefers to interact with CHO, which has a low activation free energy of 67.1 kJ mol^{-1}; thus, RCH_2CH prefers to react with CHO to realize the chain growth on Co surface, and is the reason why Co catalysts can realize the long-chain growth of C_{2+} hydrocarbons. As a result, we can predict that with the growth of carbon chain, only when the surface C_{2+} species such as RCH_2CH and RCHCH prefers to be hydrogenated to RCH_2CH_3 rather than being reacted with CH_x and CHO, can the carbon chain growth be terminated by straight alkanes, which are associated with low desorption energy. When RCHCH prefers to react with H to form $RCHCH_2$ rather than react with CH_x and CHO, and the desorption is easy, the chain growth can be terminated by straight alkenes.

3.6 General discussion

Fig. 6 presents the optimal pathway for the initiation, growth and termination of the C–C chain from syngas to CH_3CH_2CHCHO.

For the initial CH_x (x = 1–3) formation, CO prefers to be hydrogenated to CHO; starting with CHO and CHO + H, CH_x (x = 1–3) formation is easier than CH_3OH, suggesting that the Co(0001) surface exhibits good selectivity for CH_x (x = 1–3) formation rather than CH_3OH. Both CH and CH_2 are the dominant forms among all CH_x (x = 1–3) species. CH species arises from H-assisted CO dissociation, and CH_2 species is from CH hydrogenation.

For the initial C–C chain formation, CH and CH_2 species prefer to interact with CHO to give CHCHO and CH_2CHO, respectively, which are the precursors of C_2 oxygenates to realize the initial C–C chain formation. It should be noted that CHO is not thermodynamically stable on Co(0001), and is highly endothermic, which may lead to a relatively low coverage over the metal surface, and hinder its insertion reactions with CH_x

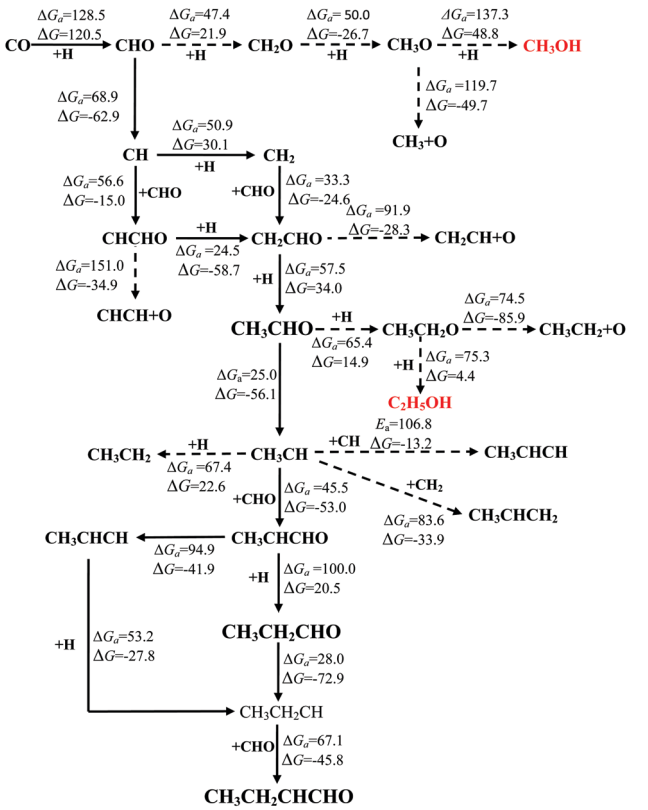

[a] Solid lines denote the main pathways in this work.
[b] E_a denotes the activation energy for the corresponding step, and ΔE represents the relevant reaction energy (unit: kJ·mol^{-1}).

Fig. 6 Schematic of the optimal reaction pathway for the initiation, growth and termination of the C–C chain from syngas at 500 K on the Co(0001) surface.

intermediates. However, Zhuo *et al.*[49] have shown that under realistic conditions, abundant hydrogen can facilitate CHO formation on the Co(0001) surface. Recently, direct evidences for CHO as the key intermediate for CO methanation was obtained by *in situ* spectroscopic experiments on supported Ru catalysts.[60] CHO insertion shows a significant superiority to CO insertion both thermodynamically and kinetically,[14,16] moreover, Xu *et al.*[16] confirmed that introducing additive Cu into Co catalyst promotes CHO formation, and facilitates C–C chain formation leading to CH_xCHO. In our studies, the chain growth also mainly depends on CHO insertion. Thus, CHO formation and stabilization on Co catalyst is important, as CHO should be the key intermediate in syngas conversion on Co catalyst, and the effect of various additives into Co catalyst on CHO formation and stabilization will be examined in our next work.

For the C–C chain growth, CHCHO and CH_2CHO prefer to be successively hydrogenated to CH_3CHO. Then, CH_3CHO prefers to dissociate into CH_3CH *via* C–O bond cleavage rather than its successive hydrogenation to ethanol, namely, the hydrogenation of aldehyde oxygenates to form an alcohol seems unlikely due to the kinetically favorable C–O bond cleavage. Subsequently, CHO insertion into CH_3CH to give CH_3CHCHO is the most favorable pathway, which realizes the successive growth of the C–C chain from C_2 to C_3 species. Further, CH_3CHCHO dissociates and hydrogenates to form CH_3CHCH and CH_3CH_2CHO, respectively. Finally, similarly to the CH_3CHO species, CH_3CH_2CHO species also prefers to dissociate into CH_3CH_2CH, and CH_3CHCH is hydrogenated to CH_3CH_2CH, then, CHO insertion into CH_3CH_2CH to provide CH_3CH_2CHCHO realizes carbon chain growth from C_3 to C_4 species.

On the basis of the above results, the comparisons among different chain growth pathways show that the CHO insertion mechanism is more preferable to realize carbon chain growth *via* either the pathway of CHO + RCH_2CH + H → RCH_2CHCHO + H → RCH_2CH_2CHO → $R'CH_2CH$ or the pathway of RCH_2CH + CHO → RCH_2CHCHO → RCH_2CHCH + H → $R'CH_2CH$, where R represents H or methyl, R′ = RCH_2. As presented in Fig. 7, the proposed propagation mechanism explicitly illustrates the initiation, growth and termination of the carbon chain from syngas on the Co(0001) surface.

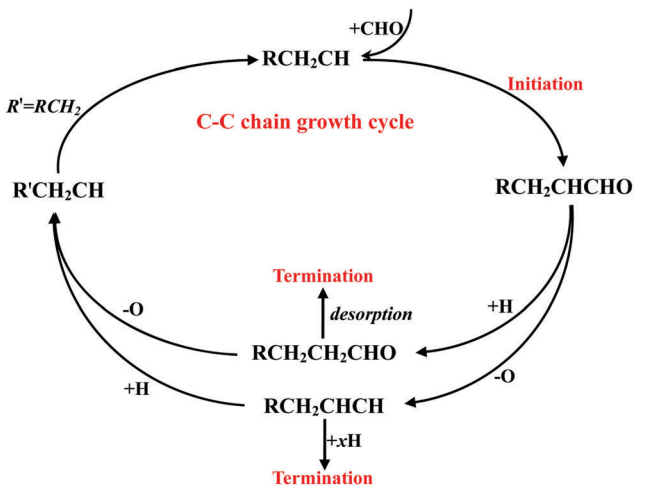

Fig. 7 The proposed mechanism for the initiation, growth and termination of the C–C chain from syngas on the Co(0001) surface. R represents hydrogen or an alkyl group.

Further, our calculated results concerning the carbon chain growth mechanism is compared with the available experimental and theoretical results. Brady *et al.*[61] have experimentally demonstrated CH_2N_2 (designed to produce CH_2) indeed couples to form C_2H_4 on Co, Fe and Ru catalysts, which supports the carbide mechanism. ^{13}C isotope tracing and NMR detection by Turner *et al.*[62] demonstrated that olefin formation is based on the alkenyl mechanism, further concluding $CH_2CH{=}CH_2$ isomerism to $CH_3CH{=}CH$, followed by the CH_2CH like species $CH_3CH{=}CH$ coupling with CH_2 to realize chain growth. Cheng *et al.*[48] have shown that the carbide mechanism is important in chain growth on both flat Co(0001) and stepped Co(0001) surfaces, then, C_2H_x + CH_x coupling reactions on the stepped Co(0001) surface[20] suggest that the CH_2 like species CH_3CH coupling with CH_2 is most favorable, further predicting that RCH + CH_2 coupling is responsible for chain growth. Zhuo *et al.*[15] have shown CO insertion into RCH to RCHCO, followed by hydrogenation steps to RCH_2CHO, subsequently, the C–O bond scission of RCH_2CHO is responsible for hydrocarbon chain formation on the Co(0001) surface. Eckle *et al.*[60] have used *in situ* spectroscopy to confirm that CHO is a key intermediate in methane formation. Zhao *et al.*[14] have performed CHO and CO insertion into CH_x on Co(0001) and Rh(111) surfaces, indicating CHO insertion is more preferable for the initial C–C chain growth than CO insertion. Xu *et al.*[16] and Zhang *et al.*[63] compared CO insertion and CHO insertion in ethanol formation from syngas on CoCu and Cu surfaces, respectively, and showed that CHO insertion is more preferable than CO insertion for the chain growth. Weststrate *et al.*[64] has confirmed the feasibility of C–O bond scission of RCH_2CHO by analyzing ethanol decomposition on the Co(0001) surface.

The above experimental and theoretical studies suggest that previous studies only focus on the partial chain growth mechanism; however, as mentioned in the Introduction, carbene coupling and CO/CHO insertion mechanisms are possible; therefore, our present studies considered and compared all possible mechanisms, from which the most favorable mechanism can be obtained, which will be more reliable and comprehensive compared to the reported studies.

For the termination of the C–C chain, this can occur at three possible positions along the growth cycle: firstly, $R'CH_2CHO$ desorption from the Co(0001) surface due to the weaker adsorption energy; secondly, the formed $R'CH_2CH$ species from $R'CH_2CHO$ dissociation is hydrogenated to alkanes; thirdly, R′CHCH with successive hydrogenation steps leads to alkanes or alkenes, which easily desorb from the Co(0001) surface. Moreover, the termination with alkanes or alkenes species will depend strongly on the hydrogen coverage on the metal surface.

Further, very low aldehyde concentrations, even compared to other oxygenates such as alcohols, are observed experimentally in FTS over supported Co catalysts,[65] which can be attributed to the low C–O dissociation energy of CH_3CHO compared to its

desorption energies. More importantly, R′CHCHO slightly prefers to dissociate into R′CHCH rather than being hydrogenated to $R'CH_2CHO$, namely, aldehydes may hardly form in FTS over supported Co catalysts.

Finally, it is worth noting that syngas conversion on Co catalysts is found to be structure sensitive,[56] the morphology of the bulk HCP Co is a dihedral-like shape with two close-packed (0001) surfaces. Moreover, the (0001) surface has a very low surface energy, and accounts for 18% of the total surface area exposed. Although, the model catalyst in this study is restricted to the Co(0001) surface it is well known that the open (10−10) and (10−11) surfaces with higher surface energies are at a higher level of 35 and 28% of the total surface area exposed, respectively. In addition, the Co(0001) surface is only a good starting point to investigate the initiation, growth and termination mechanism of the C–C chain involved in FTS on Co catalysts, and the (0001) surface is not responsible for initiation by direct C–O bond breaking as this can only be facilitated by more open facets as *e.g.* the stepped surfaces. Thus, extensive studies about the initiation, growth and termination mechanism of the C–C chain involved in FTS on Co catalysts will be considered on (10−10) and (10−11) surfaces, as well as the stepped surfaces in our next work.

4 Conclusions

In this study, the initiation, growth and termination mechanism of the C–C chain involved in Fischer–Tropsch synthesis on the Co(0001) surface have been investigated using DFT calculations. Our results show that initial CH_x (x = 1–3) formation is easier than CH_3OH formation, CH species from H-assisted CO dissociation and CH_2 species from CH hydrogenation are the dominantly existing forms of CH_x (x = 1–3) species, both CH and CH_2 species prefer to interact with CHO to form C_2 oxygenates CHCHO and CH_2CHO, which realizes the initial formation of the C–C chain; then, CHCHO and CH_2CHO prefer to be successively hydrogenated to form CH_3CHO, followed by C–O bond cleavage to give CH_3CH; subsequently, starting from CH_3CH intermediate, CHO insertion into CH_3CH can realize the further C–C chain growth to form CH_3CHCHO, followed by its dissociation and hydrogenation to give CH_3CHCH and CH_3CH_2CHO, respectively. Further, CH_3CHCH hydrogenation or CH_3CH_2CHO dissociation *via* C–O bond cleavage can form the common intermediate CH_3CH_2CH.

The mechanism of the C–C chain growth cycle has been proposed that starting from RCH_2CH, CHO insertion into RCH_2CH gives RCH_2CHCHO, followed by its hydrogenation or dissociation *via* C–O bond cleavage to give $R'CH_2CHO$ (R′ = RCH_2) or R′CHCH (R′ = RCH_2), respectively; finally, $R'CH_2CHO$ dissociation *via* C–O bond cleavage or R′CHCH hydrogenation leads to the RCH_2CH-like species $R'CH_2CH$ (R′ = RCH_2), where $R'CH_2CH$ will participate into the next C–C chain growth cycle. The C–C chain termination along the growth cycle can occur at three possible positions: $R'CH_2CHO$ desorption; $R'CH_2CH$ hydrogenated to alkanes and R′CHCH hydrogenated to alkanes or alkenes, which depend strongly on the hydrogen coverage on metal surface. Building on DFT calculations, the insights derived from this study will be valuable for both the catalyst design of Co-based and other FTS catalytic systems.

Acknowledgements

This work is financially supported by the National Natural Science Foundation of China (No. 21276003, 21476155 and 21276171), the Natural Science Foundation of Shanxi Province (No. 2014011012-2), the Program for the Top Young Academic Leaders of Higher Learning Institutions of Shanxi, and the Top Young Innovative Talents of Shanxi.

References

1 M. J. A. Tijmensen, A. P. C. Faaij, C. N. Hamelinck and M. R. M. van Hardeveld, *Biomass Bioenergy*, 2002, **23**, 129–152.
2 R. W. R. Zwart and H. Boerrigter, *Energy Fuels*, 2005, **19**, 591–597.
3 N. D. Subramanian, G. Balaji, C. S. S. R. Kumar and J. J. Spivey, *Catal. Today*, 2009, **147**, 100–106.
4 K. G. Fang, D. B. Li, M. G. Lin, M. L. Xiang, W. Wei and Y. H. Sun, *Catal. Today*, 2009, **147**, 133–138.
5 E. Iglesia, *Appl. Catal., A*, 1997, **161**, 59–78.
6 B. H. Davis, *Ind. Eng. Chem. Res.*, 2007, **46**, 8938–8945.
7 J. J. Spivey and A. Egbebi, *Chem. Soc. Rev.*, 2007, **36**, 1514–1528.
8 Y. Z. Xiang, V. Chitry, P. Liddicoat, P. Felfer, J. Cairney, S. Ringer and N. Kruse, *J. Am. Chem. Soc.*, 2013, **135**, 7114–7117.
9 K. Høydalsvik, J. B. Fløystad, A. Voronov, G. J. B. Voss, M. Esmaeili, J. Kehres, H. Granlund, U. Vainio, J. W. Andreasen, M. Rønning and D. W. Breiby, *J. Phys. Chem. C*, 2014, **118**, 2399–2407.
10 O. R. Inderwildi, S. J. Jenkins and D. A. King, *J. Phys. Chem. C*, 2008, **112**, 1305–1307.
11 M. Ojeda, R. Nabar, A. U. Nilekar, A. Ishikawa, M. Mavrikakis and E. Iglesia, *J. Catal.*, 2010, **272**, 287–297.
12 C. F. Huo, Y. W. Li, J. G. Wang and H. J. Jiao, *J. Phys. Chem. C*, 2008, **112**, 14108–14116.
13 J. Cheng, P. Hu, P. Ellis, S. French, G. Kelly and C. Martin Lok, *J. Phys. Chem. C*, 2008, **112**, 9464–9473.
14 Y. H. Zhao, K. J. Sun, X. F. Ma, J. X. Liu, D. P. Sun, H. Y. Su and W. X. Li, *Angew. Chem., Int. Ed.*, 2011, **50**, 5335–5338.
15 M. K. Zhuo, K. F. Tan, A. Borgna and M. Saeys, *J. Phys. Chem. C*, 2009, **113**, 8357–8365.
16 X. C. Xu, J. J. Su, P. F. Tian, D. L. Fu, W. W. Dai, W. Mao, W. K. Yuan, J. Xu and Y. F. Han, *J. Phys. Chem. C*, 2015, **119**, 216–227.
17 F. Fischer and H. Tropsch, *Brennst.-Chem.*, 1926, **7**, 97–104.
18 X. Q. Gong, R. Raval and P. Hu, *Surf. Sci.*, 2004, **562**, 247–256.

19 Q. F. Ge and M. Neurock, *J. Phys. Chem. B*, 2006, **110**, 15368–15380.
20 J. Cheng, P. Hu, P. Ellis, S. French, G. Kelly and C. M. Lok, *J. Catal.*, 2008, **257**, 221–228.
21 J. Gaube and H. F. Klein, *J. Mol. Catal. A: Chem.*, 2008, **283**, 60–68.
22 N. Kruse, J. Schweicher, A. Bundhoo, A. Frennet and T. V. de Bocarmé, *Top. Catal.*, 2008, **48**, 145–152.
23 S. Lin, J. Huang, X. M. Gao, X. X. Ye and H. Guo, *J. Phys. Chem. C*, 2015, **119**, 2680–2691.
24 Y. P. Pei, J. X. Liu, Y. H. Zhao, Y. J. Ding, T. Liu, W. D. Dong, H. J. Zhu, H. Y. Su, L. Yan, J. L. Li and W. X. Li, *ACS Catal.*, 2015, **5**, 3620–3624.
25 D. R. Lide and H. P. R. Frederikse, *CRC Handbook of Chemistry and Physics*, Boca Raton, FL, 1997.
26 G. A. Beitel, C. P. M. D. Groot, H. Oosterbeek and J. H. Wilson, *J. Phys. Chem. B*, 1997, **101**, 4035–4043.
27 J. P. D. Breejen, P. B. Radstake, G. L. Bezemer, J. H. Bitter, V. FroSeth, A. Holmen and K. P. de Jong, *J. Am. Chem. Soc.*, 2009, **131**, 7197–7203.
28 G. Kresse and J. Furthmuller, *Phys. Rev. B: Condens. Matter*, 1996, **54**, 11169–21118.
29 G. Kresse and J. Furthmuller, *Comput. Mater. Sci.*, 1996, **6**, 15–50.
30 P. E. Blöchl, *Phys. Rev. B: Condens. Matter*, 1994, **50**, 17953–17979.
31 G. Kresse and D. Joubert, *Phys. Rev. B: Condens. Matter*, 1999, **59**, 1758–1775.
32 J. P. Perdew, J. A. Chevary, S. H. Vosko, K. A. Jackson, M. R. Pederson, D. J. Singh and C. Fiolhais, *Phys. Rev. B: Condens. Matter*, 1992, **46**, 6671–6687.
33 S. G. Louie, S. Froyen and M. L. Cohen, *Phys. Rev. B*, 1982, **26**, 1738–1742.
34 Q. Ge, M. Neurock, H. A. Wright and N. Srinivasan, *J. Phys. Chem. B*, 2002, **106**, 2826–2829.
35 L. Joos, I. A. W. Filot, S. Cottenier, E. J. M. Hensen, M. Waroquier, V. V. Speybroeck and R. A. van Santen, *J. Phys. Chem. C*, 2014, **118**, 5317–5327.
36 Y. H. Zhao, M. M. Yang, D. P. Sun, H. Y. Su, K. J. Sun, X. F. Ma, X. H. Bao and W. X. Li, *J. Phys. Chem. C*, 2011, **115**, 18247–18256.
37 J. J. Plata, V. Collico, A. M. Marquez and J. F. Sanz, *Theor. Chem. Acc.*, 2013, **132**, 1311.
38 D. C. Sorescu, J. Lee, W. A. Al-Saidi and K. D. Jordan, *J. Chem. Phys.*, 2011, **134**, 104707.
39 T. Lu and F. W. Chen, *J. Mol. Model.*, 2013, **19**, 5387–5395.
40 D. Sheppard, P. Xiao, W. Chemelewski, D. D. Johnson and G. Henkelman, *J. Chem. Phys.*, 2012, **136**, 074103.
41 D. Sheppard, R. Terrell and G. Henkelman, *J. Chem. Phys.*, 2008, **128**, 134106.
42 G. Henkelman and H. Jónsson, *J. Chem. Phys.*, 1999, **111**, 7010–7022.
43 R. A. Olsen, G. J. Kroes, G. Henkelman, A. Arnaldsson and H. Jónsson, *J. Chem. Phys.*, 2004, **121**, 9776–9792.
44 X. M. Cao, R. Burch, C. Hardacre and P. Hu, *Catal. Today*, 2011, **165**, 71–79.
45 A. Y. Khodakov, *Catal. Today*, 2009, **144**, 251–257.
46 R. G. Zhang, G. R. Wang and B. J. Wang, *J. Catal.*, 2013, **305**, 238–255.
47 W. X. Pan, R. Cao and G. L. Griffin, *J. Catal.*, 1988, **114**, 447–456.
48 J. Cheng, X. Q. Gong, P. Hu, C. Martin Lok, P. Ellis and S. French, *J. Catal.*, 2008, **254**, 285–295.
49 M. K. Zhuo, A. Borgna and M. Saeys, *J. Catal.*, 2013, **297**, 217–226.
50 J. P. Clay, J. P. Greeley, F. H. Ribeiro, W. N. Delgass and W. F. Schneider, *J. Catal.*, 2014, **320**, 106–117.
51 B. Jiang, X. X. Hu, S. Lin, D. Q. Xie and H. Guo, *Phys. Chem. Chem. Phys.*, 2015, **17**, 23346–23355.
52 S. Shetty and R. A. van Santen, *Catal. Today*, 2011, **171**, 168–173.
53 A. M. L. Øiestad and E. Uggerud, *Chem. Phys.*, 2000, **262**, 169–177.
54 J. Nerlov, S. Sckerl, J. Wambach and I. Chorkendorff, *Appl. Catal., A*, 2000, **191**, 97–109.
55 F. Studt, F. A. Pedersen, Q. X. Wu, A. D. Jensen, B. Temel, J. D. Grunwaldt and J. K. Nørskov, *J. Catal.*, 2012, **293**, 51–60.
56 J. X. Liu, H. Y. Su, D. P. Sun, B. Y. Zhang and W. X. Li, *J. Am. Chem. Soc.*, 2013, **135**, 16284–16287.
57 G. Prieto, A. Martínez, P. Concepción and R. Moreno-Tost, *J. Catal.*, 2009, **266**, 129–144.
58 T. Anders, C. Sophie, C. Mahati, C. Cheng-Hao, E. Carlos, P. Elzbieta, J. Peng, B. Ferenc, B. Brandon and A. A. Paul, *J. Am. Chem. Soc.*, 2013, **135**, 519.
59 J. Yang, Y. Y. Qi, J. Zhu, Y. A. Zhu, D. Chen and A. Holmen, *J. Catal.*, 2013, **308**, 37–49.
60 S. Eckle, H. G. Anfang and R. J. Behm, *J. Phys. Chem.*, 2010, **115**, 1361–1367.
61 R. C. Brady and R. Pettit, *J. Am. Chem. Soc.*, 1980, **102**, 6181–6182.
62 M. L. Turner, H. C. Long, A. Shenton, P. K. Byers and P. M. Maitlis, *Chem.–Eur. J.*, 1995, **1**, 549–556.
63 R. G. Zhang, X. C. Sun and B. J. Wang, *J. Phys. Chem. C*, 2013, **117**, 6594–6606.
64 C. J. Weststrate, H. J. Gericke, M. W. G. M. Verhoeven, I. M. Ciobîcă, A. M. Saib and J. W. Niemantsverdriet, *J. Phys. Chem. Lett.*, 2010, **1**, 1767–1770.
65 M. E. Dry, *Appl. Catal., A*, 1996, **138**, 319–344.